Limitation by vapour pressure deficit shapes different intra-annual growth patterns of diffuse- and ring-porous temperate broadleaves

Jan Tumajer[1,2] (iD), **Tobias Scharnweber[1]** (iD), **Marko Smiljanic[1]** (iD) and **Martin Wilmking[1]** (iD)

[1]Institute of Botany and Landscape Ecology, University of Greifswald, Soldmannstraße 15, 17487 Greifswald, Germany; [2]Department of Physical Geography and Geoecology, Faculty of

Science, Charles University, Albertov 6, 12843 Prague, Czech Republic

Author for correspondence:
Jan Tumajer
Email: tumajerj@uni-greifswald.de

Summary

- Understanding the effects of temperature and moisture on radial growth is vital for assessing the impacts of climate change on carbon and water cycles. However, studies observing growth at sub-daily temporal scales remain scarce.
- We analysed sub-daily growth dynamics and its climatic drivers recorded by point dendrometers for 35 trees of three temperate broadleaved species during the years 2015–2020. We isolated irreversible growth driven by cambial activity from the dendrometer records. Next, we compared the intra-annual growth patterns among species and delimited their climatic optima.
- The growth of all species peaked at air temperatures between 12 and 16°C and vapour pressure deficit (VPD) below 0.1 kPa. *Acer pseudoplatanus* and *Fagus sylvatica*, both diffuse-porous, sustained growth under suboptimal VPD. Ring-porous *Quercus robur* experienced a steep decline of growth rates with reduced air humidity. This resulted in multiple irregular growth peaks of *Q. robur* during the year. By contrast, the growth patterns of the diffuse-porous species were always right-skewed unimodal with a peak in June between day of the year 150–170.
- Intra-annual growth patterns are shaped more by VPD than temperature. The different sensitivity of radial growth to VPD is responsible for unimodal growth patterns in both diffuse-porous species and multimodal growth pattern in *Q. robur*.

Introduction

Woody plants respond to climate change by alteration of physiological processes at various temporal scales (Becklin *et al.*, 2016). The unprecedented pace of climate change might exceed the species-specific capacity for physiological adjustments, leading to the disruption of long-standing ecological patterns of niche distribution, climate–growth interaction and natural selection (Körner, 2018). The existence of feedback mechanisms between plant physiology and the climatic system (Peñuelas *et al.*, 2009) increases the need for a mechanistic understanding of environmental effects on plant growth. For instance, variations in intra-annual cambial activity, specifically the production and maturation of new xylem and phloem cells, exert control over the carbon sequestration capacity of the entire ecosystems dominated by woody species (Pan *et al.*, 2011; Cuny *et al.*, 2015). Although shifting climatic limitation of annual growth rates has recently been described using tree-ring widths across space (Babst *et al.*, 2019; Cook *et al.*, 2020) and over time (Wilmking *et al.*, 2020),

the understanding of high-frequency variability in sub-daily growth rates is limited (but see Zweifel *et al.*, 2021).

The radial growth rate is assumed to reflect the variability of the most limiting climatic factor during a specific part of the growing season (Vaganov *et al.*, 2006). The onset and kinetics of cambial activity in cold environments tend to follow the intra-annual pattern of air temperature and photoperiod (Deslauriers *et al.*, 2008; Rossi *et al.*, 2016; Huang *et al.*, 2020). Indeed, boreal and mountain forests show a single distinct peak of growth rates around the summer solstice (Rossi *et al.*, 2003). In dry ecosystems, by contrast, tree-ring formation might be restricted to discontinuous windows with sufficient moisture availability (Ziaco & Biondi, 2018; Güney *et al.*, 2020). Consequently, bimodal or multimodal intra-annual growth patterns predominate in Mediterranean biomes (Cherubini *et al.*, 2003; Campelo *et al.*, 2018) and semi-arid environments (Wu *et al.*, 2020; Morino *et al.*, 2021). Joint control of and periodic switching between dominant effects of temperature and moisture availability during the year can be assumed in mesic

environments such as European broadleaved temperate forests (Siegmund *et al.*, 2016).

Moreover, radial growth patterns might vary between the species inhabiting this ecosystem owing to marked between-species differences in drought susceptibility (Lévesque *et al.*, 2013; Vanhellemont *et al.*, 2019; Grossiord *et al.*, 2020). However, species' sensitivity to drought possibly differs with respect to considered temporal scale of drought effects (annual vs sub-daily). Ring-porous broadleaves with large differences in wood anatomy between earlywood and latewood experience a longer growing season, so they can form the earlywood part of the annual tree-ring in early spring, with a low probability of drought stress (Sass-Klaassen *et al.*, 2011; Pérez-de-Lis *et al.*, 2016). By contrast, the annual growth rate of diffuse-porous species with a homogeneous wood structure is more dependent on the summer dry season as a result of a delayed cambial activity onset (Prislan *et al.*, 2013). Consequently, greater sensitivity of annual growth rates to drought has repeatedly been reported for diffuse- compared to ring-porous species (Scharnweber *et al.*, 2011; Vanhellemont *et al.*, 2019). On a sub-daily scale, however, ring-porous broadleaves with large conduits are more prone to cavitation-induced embolism which might limit radial growth during days with strong negative water potential (Pallardy, 2008; Sperry *et al.*, 2008). Diffuse-porous broadleaves prevent cavitation by closing their stomata early, which might also restrict radial growth during dry periods through a drop in photosynthetic rates or even carbon starvation (Backes & Leuschner, 2000; Scherrer *et al.*, 2011; Walthert *et al.*, 2021). Probably as a result of this, an analysis of hourly growth rates on diurnal scale revealed similar and robust growth responses to drought with indistinct deviations between species regardless of the type of wood anatomy (Zweifel *et al.*, 2021).

Reliable information about high-frequency variability of the stem radius and its climatic drivers can be provided by point dendrometers (Drew & Downes, 2009). Dendrometer data can be used to assess the effects of recent unprecedented climatic conditions on radial growth patterns (Campelo *et al.*, 2018; Scharnweber *et al.*, 2020; Krejza *et al.*, 2021) and to link them with current shifts in biochemical cycles and the health status of forest ecosystems (Ciais *et al.*, 2005; Camarero *et al.*, 2015; Anderegg *et al.*, 2016). However, linking stem radius variability recorded by dendrometers with climatic conditions is not straightforward. The signal of the radial stem growth – i.e. irreversible stem radial variation – in dendrometer records is masked by additional processes reversibly altering the instant stem radius. For instance, stem shrinkage caused by variable tree-water deficit (Zweifel *et al.*, 2005; Güney *et al.*, 2020) or winter freezing–thawing cycles of intercellular water (Zweifel & Häsler, 2000) often accounts for the largest part of stem radius variability. Because water availability affects both reversible and irreversible radial stem changes, actual growth needs to be isolated from total variability before its climatic drivers can be assessed (Zweifel *et al.*, 2016).

In this study, we used six years of radial growth data with 30-min resolution for three coexisting broadleaved temperate species (*Quercus robur* L., *Fagus sylvatica* L., *Acer pseudoplatanus* L.) to identify the interacting effect of moisture availability and temperature on their radial stem growth. We isolated the part of radial

stem variability attributable to irreversible growth (Zweifel *et al.*, 2016) and analysed its intra-annual pattern. We calculated skewness, kurtosis, and employed Hartingan's and Silverman's bimodality tests to distinguish trees, species and years with unimodal and multimodal patterns of growth rates during the growing season. In addition, we fitted linear mixed-effects models to quantify the contribution of the main climatic variables and various sources of random variability for intra-annual growth rates of each species. We hypothesized that growth rates variability can be statistically predicted by a combination of climatic variables related to air temperature and moisture availability (Zweifel *et al.*, 2021). In addition, we assumed that *Q. robur*, owing to its larger conduits prone to cavitation (Sperry *et al.*, 2008), will show a greater dependence of growth on moisture availability and a stronger tendency towards drought-induced growth multimodality compared to *A. pseudoplatanus* and *F. sylvatica* with small conduits.

Materials and Methods

Study area and experimental design

We analysed data from three permanent ecological monitoring plots which form part of the LTER-D network situated in northeastern Germany near the town of Greifswald (54.077°N, 13.455°E; Fig. 1a). The climate in the study area is temperate humid with a long-term mean annual temperature of 8.5°C and mean annual precipitation of 580 mm (DWD Greifswald meteorological station). Monitoring of stem radius was initiated between 2013 and 2016 and has been performed continuously since that time (van der Maaten *et al.*, 2018; Scharnweber *et al.*, 2020). The dendrometers Type DR1 (Ecomatik, Dachau/Munich, Germany) connected to a CR1000 logger in Full Bridge configuration are used to record stem radius variability in a 5-min timestamp for *Q. robur* (13 trees), *F. sylvatica* (15 trees) and *A. pseudoplatanus* (seven trees). Each individual tree has its own logger in two of the inland plots and one logger records five dendrometers (maximum cable length of 20 m) in a centralized setup at the Vilm island plot (Fig. 1a). For this study, we subsampled the time series to 30-min resolution. The outermost layer of *Q. robur* bark was removed before installing the dendrometers to minimize the distortion of the growth signal by the hygroscopic shrinking and swelling of the bark tissue. In addition to dendrometer data, *in situ* recordings of micrometeorological and soil moisture variables were performed using HC2S3 and CS655 sensors (Campbell Scientific, Logan, UT, USA) (Fig. 1b). Although the distance between plots is *c.* 30 km and plots differ in soil conditions and management history, radial growth dynamics are very similar among the sites (Scharnweber *et al.*, 2020). We therefore pooled the data from different plots together and treated them as a single dataset.

Separation of irreversible growth and reversible variability in stem radius dynamics

In the initial step, we performed a visual quality check of all datasets and removed apparently incorrect data resulting from
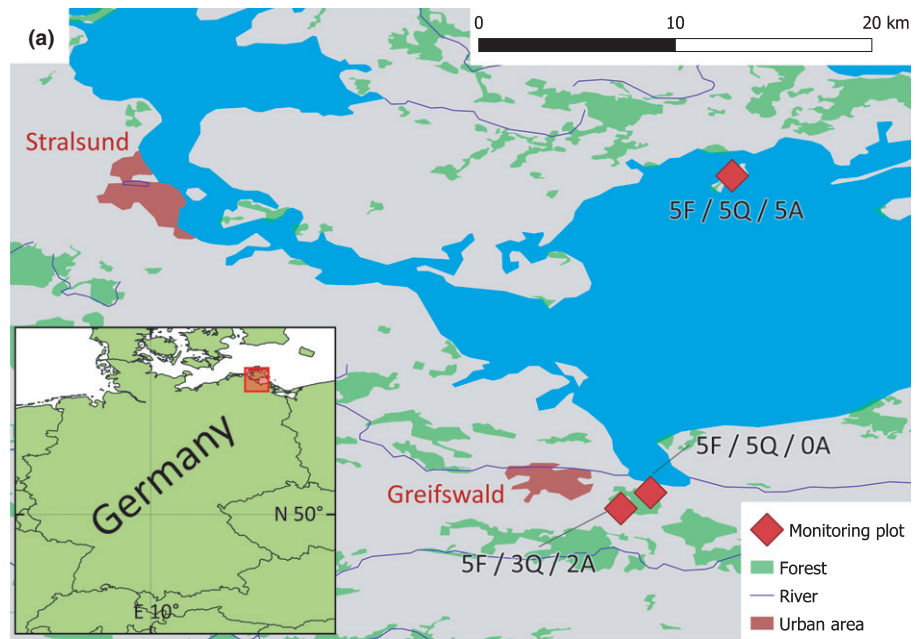
Fig. 1 Location of monitoring plots in north-eastern Germany (a). Codes next to each plot indicate numbers of monitored individuals of *Fagus sylvatica* (F), *Quercus robur* (Q), and *Acer pseudoplatanus* (A). The forest extent is according to CORINE Land Cover data. Mean intra-annual variability of air temperature (red), volumetric soil water content at 0.2 m depth (blue), relative air humidity (green) and vapour pressure deficit (orange) during 2015–2020 averaged for all sites (b). The buffer indicates $\pm 0.5 \times$ standard deviation among individual years for the given day of the year (DOY).
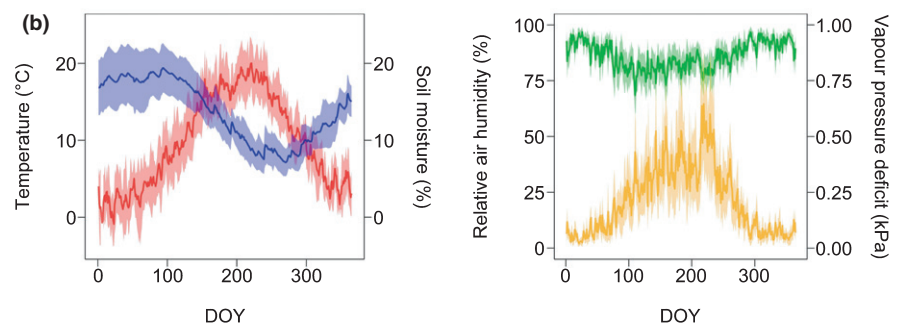
temporary sensor failures. As we focused on the effect of weather conditions on irreversible radial growth, we primarily had to filter out reversible stem radial dynamics driven mainly by variation in the amount and state of internal stem water (Zweifel & Häsler, 2000; Deslauriers *et al.*, 2007; King *et al.*, 2013). To do so, we followed the 'zero-growth approach' to distinguish between reversible and irreversible processes affecting the stem radius (Zweifel *et al.*, 2016). We ascribed the entire variability in stem radius below the previous stem radius maximum to reversible shrinking and swelling driven by tree-water deficit, while all the variability exceeding the previous stem radius maximum was regarded as irreversible growth due to cambial activity (GRO rate):

$$\text{GRO rate}_{t,m}$$
$$= \begin{cases} 0, & \text{if } R_{t,m} \leq \max R_{t,1}; R_{t,(m-1)} \\ R_{t,m} - \max R_{t,1}; R_{t,(m-1)}, & \text{if } R_{t,m} > \max R_{t,1}; R_{t,(m-1)} \end{cases}$$
$$\text{Eqn 1}$$

where R indicates the stem radius recorded by the dendrometer, t indicates a tree, and m indicates the order of 30-min timestamps. The GRO rate captured by dendrometers is driven mainly by processes of cambial cells' division and radial lumen enlargement but does not reflect cell wall lignification and maturation (Cuny

et al., 2015). To filter out unrealistic observations possibly caused by sensor artefacts, we removed all timestamps with GRO rates greater than 100 μm per 30 min. However, this affected only 64 of > 4 000 000 timestamps.

In addition to the continuous GRO rate variable, we defined a GRO occurrence binary variable, which for each 30-min timestamp indicates whether growth occurred (i.e. GRO rate > 0 μm h^{-1}) or not (i.e. GRO rate = 0 μm h^{-1}). Moreover, we standardized GRO rate at each timestamp by the cumulative annual GRO rate of a specific tree during the main part of the growing season to determine the relative GRO contribution of each timestamp to annual growth. The main growing season was defined as the period between day of the year (DOY) 80 and 320 (late March to mid-September). The main growing season excludes winter months when the stem diameter can be significantly affected by freezing–thawing cycles of internal water (Zweifel & Häsler, 2000) but covers the entire period of radial growth expected in our study region (van der Maaten *et al.*, 2018).

Visualization and statistical analysis of intra-annual growth patterns

The time series of GRO variables were used to visualize intra-annual and diurnal patterns of radial growth and to assess their

variability between years, species and trees. We aggregated GRO variables from 30-min resolution to a daily scale for each species and year. Specifically, we determined the mean daily GRO rate and the proportion of trees which experienced at least one timestamp with GRO occurrence during the day (i.e. at least one 30-min timestamp during the day with GRO rate > 0 µm h^{-1}) for each species and year. To highlight the overall intra-annual pattern of daily GRO rates, we smoothed the variability using a spline with 25 degrees of freedom. In addition to describing intra-annual variability of daily-resolved GRO variables, we also assessed diurnal (00:00–23:59) pattern of 30-min-resolved GRO rates. To do so, we averaged GRO rate for each half-hourly segment of the diurnal cycle across different days of the year for each species.

To quantify deviations of the intra-annual growth patterns from a theoretical symmetrical distribution with a single dominant peak (Rossi *et al.*, 2003), we calculated skewness and kurtosis of smoothed daily GRO rates during the main growing season for each species and year. Low values of kurtosis indicate a flat distribution with a marginal peak, while positive (negative) values of skewness indicate shifting of the peak to the early (late) part of the growing season. The distribution multimodality of smoothed GRO rates during the main growing season was tested for each species and year using Hartingan's dip test (Kang & Noh, 2019) and Silverman's critical bandwidth test (Silwerman, 1981). Hartingan's dip test evaluates the hypothesis that the given data have more than one mode in the distribution (multimodal distribution) employing the 'dip' statistic, which represents the maximum difference between the empirical distribution and its optimal theoretical unimodal approximation. Silverman's bandwidth test is based on the minimal size of the bandwidth required to observe one mode in the distribution smoothed by the Gaussian kernel function. In addition to testing the distribution multimodality of the mean GRO rate for each species and year, we also tested the multimodality of the mean GRO rates for each tree.

Climate–radial growth interaction

We employed different statistical and visual approaches to highlight and quantify the independent and combined effects of environmental factors on GRO variables. The analysis included the following environmental variables, which were measured *in situ* with 30-min resolution: air temperature (°C) and relative air humidity (%) at 2 m height, and the volumetric water content at 0.2 m depth (%). In addition, we calculated the time series of vapour pressure deficit (VPD; kPa) in 30-min resolution from relative air humidity and temperature using the approach described in Duursma (2015).

All statistics described later were calculated for data with 30-min resolution at the level of individual trees and, afterwards, summarized at the species level (using the mean and/or standard deviation of statistics between trees). Initially, we correlated GRO rates with environmental variables during the respective 30-min interval. To reveal an intra-annual pattern, we calculated correlations separately for each calendar month. Next, we

converted continuous environmental variables into categorial variables to ascertain mean values of GRO variables during specific intervals of environmental conditions over the main growing season (DOY 80–320) for each species. Individual intervals of environmental variables had a step of 2°C (temperature), 0.1 kPa (VPD) and 2.5% (air humidity and soil moisture). We calculated the mean GRO rates, the proportions of timestamps with GRO occurrence out of the total number of timestamps with growth, and the cumulative GRO contribution to total annual growth for each interval of environmental variables. We compared the proportions of GRO occurrence and contribution for each interval with frequency of specific environmental conditions to highlight intervals with growth below or above the frequency of such conditions. Finally, we plotted two-dimensional frequency scatterplots showing the mean GRO rate, occurrence and contribution per each specific combination of the two most influential environmental variables. Because both the correlation analysis and histograms pointed to joint dominant growth control by air temperature and VPD, we used this pair of variables in all scatterplots.

We employed generalized linear mixed-effects models to quantify the relative contributions of the environmental variables and various sources of independent variability on GRO rate, GRO occurrence and GRO contribution to annual growth. The models were fit for the 30-min timestamps from the main part of the growing season (DOY 80–320). The model structure tested for various sources of temporal and between-tree variability in GRO variables, specifically (1) direct effects of temperature and VPD on GRO variables; (2) between-tree differences in mean GRO variables and in sensitivity to temperature and VPD; and (3) between-year differences in mean GRO variables. The model structure was as follows:

$$\left.\begin{array}{l} \text{GRO rate}_{t,m,y} \\ \text{GRO occur}_{t,m,y} \\ \text{GRO contrib}_{t,m,y} \end{array}\right\} = \beta_0 + \beta_1 \cdot \text{Temp}_m + \beta_2 \cdot \text{VPD}_m + U_{0a}(t)$$
$$+ U_1(t) \cdot \text{Temp}_m + U_2(t) \cdot \text{VPD}_m + U_{0b}(y)$$
Eqn 2

where β_0 represents a fixed intercept, β_{1-2} represent fixed slopes of environmental variables, U_{0a-0b} represent random intercepts for each tree and year, U_{1-2} represent random slopes of environmental variables for each tree, t stands for a tree, m stands for timestamp with 30-min resolution, and y stands for a year. The models were fit separately with the same structure for each species (i.e. three response variables × three species = nine models were fit in total). The same structure of the model was applied for all response variables accounting for their different distribution (Gaussian for GRO rate and contribution, and binomial for GRO occurrence). The quality of the models was assessed by marginal (R^2m) and conditional (R^2c) pseudo-R^2 statistics (Nakagawa & Schielzeth, 2013). During the model interpretation, we specifically focused on the following five questions: Q1: What is the level of temporal and between-tree heterogeneity in GRO variables in comparison to the direct climatic forcing? (i.e.

comparison of R^2c and R^2m); Q2: Is the combined effect of temperature and VPD on GRO variables positive or negative? (i.e. are $\beta_1 + U_1$ and $\beta_2 + U_2$ positive or negative?); Q3: Is the level of temporal heterogeneity higher compared to between-tree heterogeneity? (i.e. comparison of random variances accounted for by U_{0a} and U_{0b}); Q4: Is the between-tree heterogeneity of GRO variables greater in response to temperature compared to VPD? (i.e. comparison of random variances accounted for by U_1 and U_2); Q5: Which years experienced suboptimal conditions for GRO? (i.e. which years have negative U_{0b}?).

All analyses were based on the period from 1 January 2015 to 31 December 2020 to maximize the number of trees with available observations. All steps of the data processing, statistical analyses and visualization were performed in R (R Core Team, 2020), utilizing the packages 'LMER' (mixed-effects models; Bates *et al.*, 2015), 'MULTIMODE' (modality tests; Ameijeiras-Alonso *et al.*, 2021), 'PLANTECOPHYS' (VPD calculation; Duursma, 2015) and 'GGPLOT2' (charts' plotting; Wickham, 2009).

Results

The intra-annual patterns of daily GRO rates varied both among species and years (Fig. 2). The highest GRO rate peaks were documented for *A. pseudoplantanus* whereas *Q. robur* experienced the lowest growth rates. Mean daily GRO rates of *Q. robur* exhibited the lowest kurtosis of all the species each year, suggesting a lesser dominance of the global optimum and spread across the longest duration of the growing season. By contrast, high values of both skewness and kurtosis reflected the existence of a single peak around DOY 150–170 in both diffuse-porous species. Both bimodality tests confirmed a unimodal distribution for the diffuse-porous species in most years. The tests, however, failed to identify a clear peak in the daily GRO rate distribution in five of the six years for *Q. robur*. Only in 2020, the existence of the single global maximum in the distribution was confirmed statistically; however, the GRO rate pattern visually showed the existence of additional local maxima in the distribution. The tree-specific intra-annual growth patterns of *Q. robur* had the
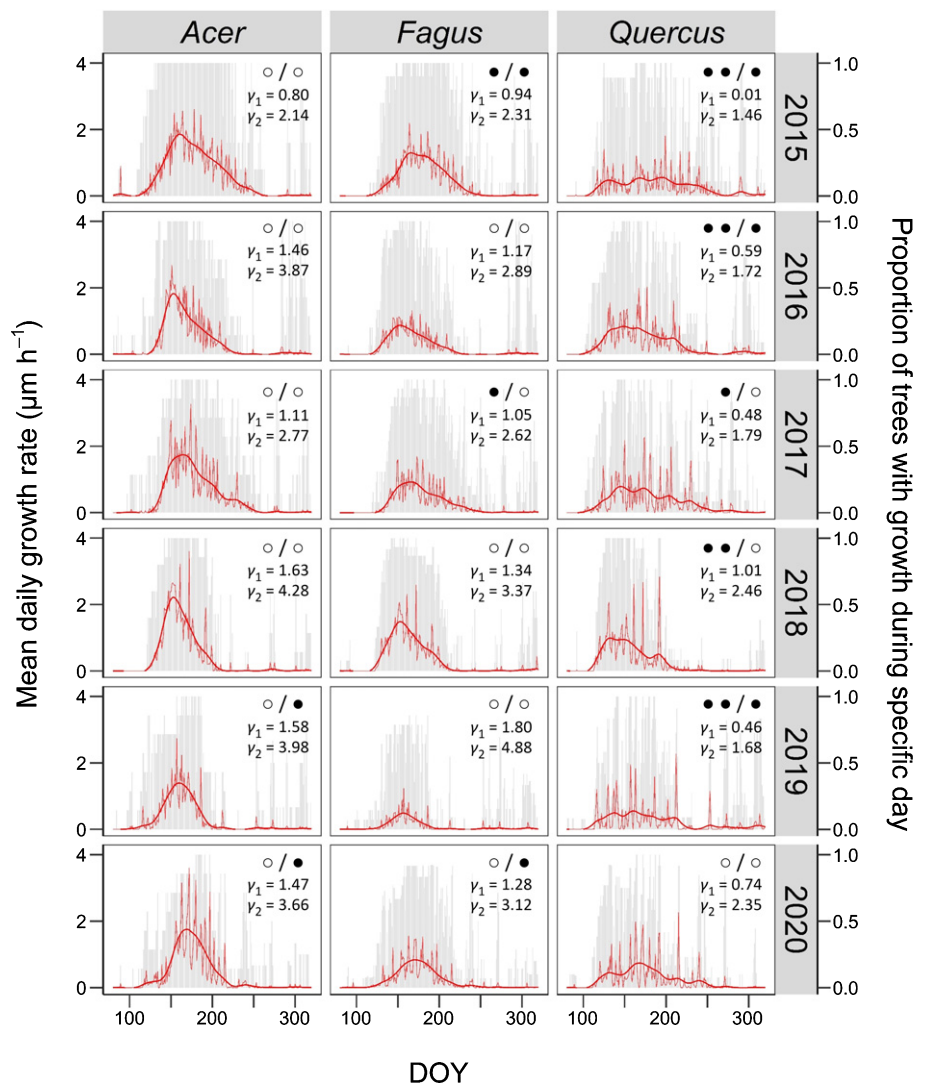
Fig. 2 Mean daily growth rates determined by the zero-growth approach (red lines), their overall intra-annual pattern estimated as a spline with 25 degrees of freedom (bold red lines) and proportions of trees that experienced growth during specific day of the year (DOY) (grey bars). The dots indicate significance levels of Hartingan's dip tests/Silverman's bandwidth tests of distribution multimodality (empty dot (○) = $P > 0.05$, single full dot (●) = $P < 0.05$, double full dot (●●) = $P < 0.01$). The γ_1 and γ_2 are distribution skewness and kurtosis, respectively.

lowest mean kurtosis and skewness, and most of them were significantly multimodal according to both tests (Supporting Information Table S1). In addition, only Silverman's test pointed towards frequent bimodality of individual *F. sylvatica* trees. The daily proportions of trees with GRO occurrence experienced rather continuous shifts during the growing season in diffuse-porous broadleaves (increasing mainly before DOY 150, stable high during DOY 150–180 and declining afterwards with marked intra-annual variability of those phases). By contrast, the proportion of growing trees was greatly variable from day to day in *Q. robur* (Fig. 2).

The results of the correlation analysis between the GRO rate and environmental variables at 30-min resolution were similar among the species (Fig. 3). The strongest correlations occurred between the GRO rate and May-August relative air humidity (positive) and May–August VPD (negative). In addition, the GRO rate correlated negatively with air temperature during the June–July period. In contrast to variables related to water vapour and temperature, the correlations with volumetric soil moisture content were weak. The only remarkable difference between the species was related to stronger positive May correlations with temperature and weaker negative correlations with May moisture availability for *Q. robur* compared to other species. The mean GRO rate was the highest in the intervals of air temperature of 10–20°C, VPD of 0–0.1 kPa and relative air humidity of 97.5–100% (Fig. 4a). The distribution of days with GRO occurrence and GRO contribution to annual growth mirrored the pattern of GRO rates, with additional remarkable peak for *A. pseudoplatanus* in the interval of soil moisture content of 0–5% (Fig. 4b,c). The difference between GRO contribution to annual growth and the air temperature distribution was the highest for the interval of 12–18°C. Whereas temperatures fell within this interval at 41% of timestamps, cumulative growth during those conditions represented between 64% (*Q. robur*) and 78% (*A. pseudoplatanus*) of the total growth during the 2015–2020 period. In addition, the GRO contribution to the annual growth of *Q. robur* largely lagged the frequency of timestamps for intervals with low relative

air humidity and high VPD. Specifically, whereas diffuse-porous species produced 48–53% of annual cumulative growth in conditions with VPD > 0.1 kPa, this interval contributed only 32% for *Q. robur*. All GRO variables quickly dropped with increasing VPD above 0.1 kPa for all species, but mainly *Q. robur*, and became marginal above 0.5 kPa.

All species experienced the highest GRO rates, occurrence and contribution to total growth in the cases of 30-min intervals with temperatures close to 12–16°C and VPD ≤ 0.1 kPa (Fig. 5). All GRO variables tended to decline towards both higher and lower temperatures as well as towards higher VPD. The observed distribution of GRO variables across temperature–VPD space showed only marginal variability between the species and over time (Fig. S1–S3). The GRO rate of all the species peaked mostly at night (between 20:00–6:00) but was limited during the day (Fig. S4).

Conditional R^2, R^2c, of mixed-effects models explaining GRO variables at 30-min resolution spanned the ranges 0.58–0.70, 0.58–0.93 and 0.40–0.53 for models of GRO rate, GRO occurrence and GRO contribution, respectively (Table 1). For all the models, R^2c significantly exceeded marginal R^2, R^2m, (0.01–0.24) indicating strong between-tree and temporal variability in GRO response to the climate (a priori defined Q1 tested by the model). The combined effects (fixed + random effects between trees) on all GRO variables were always negative in the case of VPD but positive in the case of temperature (Table S2). This indicates a negative response of growth to increasing VPD but an overall positive response to increasing temperature. Specifically, GRO rates dropped between −0.14 and −1.09 μm h^{-1} kPa^{-1} but rose between 0.005 and 0.055 μm h^{-1} °C^{-1}, respectively (Q2). Negative random intercepts for years highlighted suboptimal GRO rates in 2019 and 2020 for all species and in 2016 for *A. pseudoplatanus* and *F. sylvatica* (Table S3; Q5). Random variance of the intercept was greater between trees compared to between years in 56% of models (=5/9), suggesting that GRO variability among trees slightly outweighs variability over time (Q3). The variance between trees in VPD slope was always
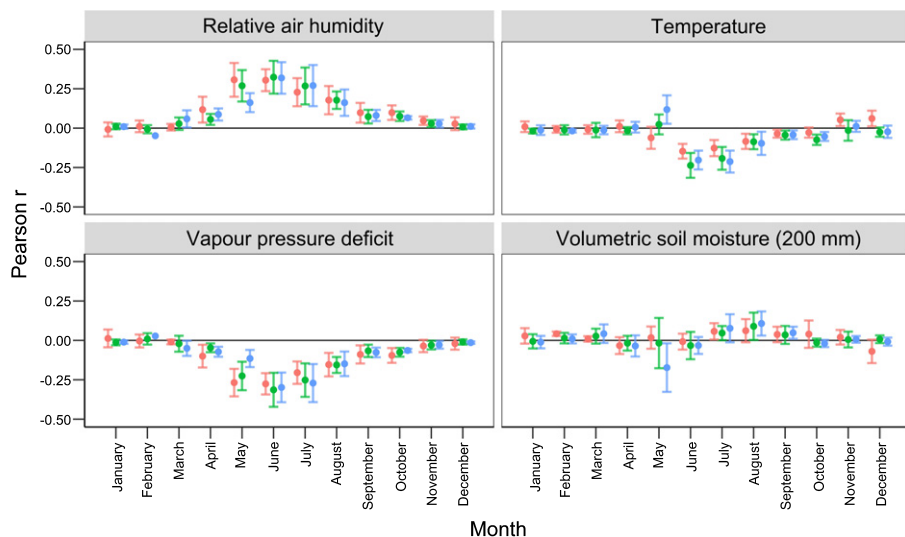
Fig. 3 Correlation coefficients between climatic conditions and radial growth rates of 30-min timestamps during specific calendar months. Points represent mean values of correlation coefficients of all trees; error lines show ± standard deviation of individual trees correlations. Colours indicate *Acer pseudoplatanus* (red), *Fagus sylvatica* (green) and *Quercus robur* (blue).
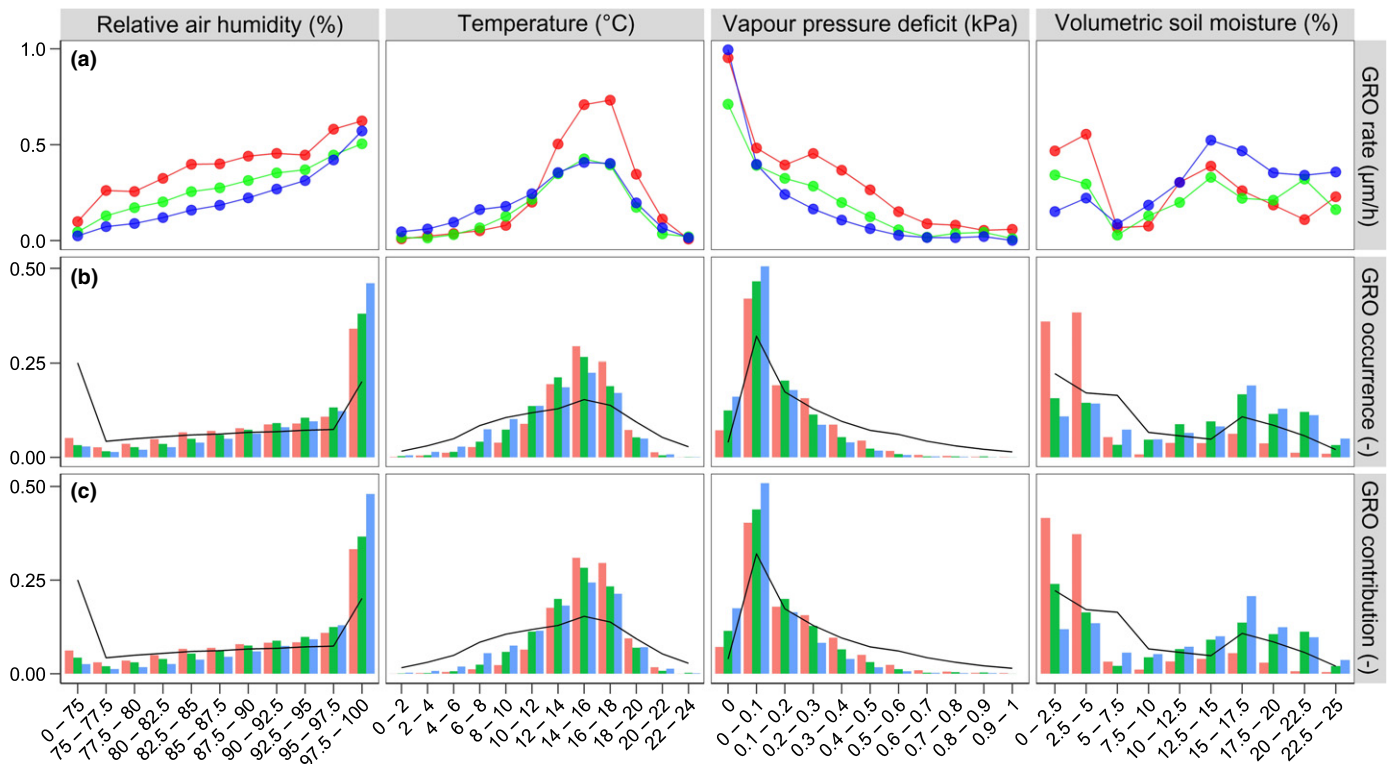
Fig. 4 Mean radial growth rates (a, top row), the proportion of timestamps with growth occurrence out of the total number of timestamps with growth (b, middle row), and the proportion of cumulative growth on total cumulative growth (c, bottom row) during specific intervals of environmental conditions. Black lines in bar charts indicate the frequency distribution of 30-min timestamps with specific environmental conditions. Colours indicate *Acer pseudoplatanus* (red), *Fagus sylvatica* (green) and *Quercus robur* (blue).
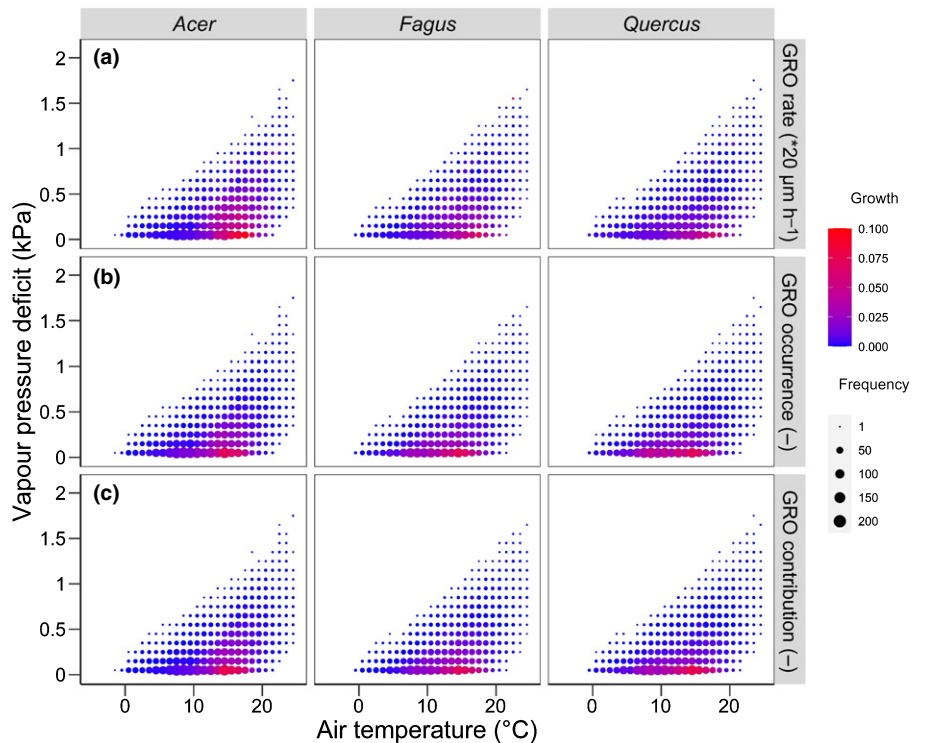
Fig. 5 Scatterplots of air temperatures and vapour pressure deficits for the period 2015–2020. The size of dots indicates the frequency of 30-min timestamps per tree and year with specific climatic conditions. The colour scale indicates a mean rate of radial growth (a), the proportion of timestamps with growth occurrence out of the total number of timestamps with growth (b), and contribution of growth to total cumulative growth (c) during specific climatic conditions. Individual points represent 1°C × 0.1 kPa intervals. Note the different unit scale applied in (a).

Table 1 Results of mixed-effects models predicting the occurrence, contribution and rate of radial growth.

Species	GRO independent variable	Fixed effects estimates			Random effects variance					R^2m	R^2c
		Int	Temp	VPD	Int|Tree	VPD|Tree	Temp|Tree	Int|Year	Residual		
Acer	Occurrence (−)	−3.667	0.181	−5.782	0.247	5.536	0.002	0.332		0.24	0.58
	Rate (µm h^{-1})	−0.065	0.031	−0.582	0.956	0.984	0.004	0.841	0.656	0.01	0.68
	Contribution (× 10^{-4})	0.158	0.177	−4.111	0.034	> 0.001	> 0.001	0.001	0.016	0.01	0.47
Fagus	Occurrence (−)	−2.900	0.159	−6.682	2.169	2.963	0.002	0.474		0.07	0.93
	Rate (µm h^{-1})	0.013	0.020	−0.411	0.164	0.040	> 0.001	0.286	0.328	0.02	0.58
	Contribution (× 10^{-4})	−0.233	0.181	−4.011	0.001	> 0.001	> 0.001	0.014	0.013	0.01	0.53
Quercus	Occurrence (−)	−2.588	0.127	−7.389	1.224	2.276	0.002	0.164		0.13	0.89
	Rate (µm h^{-1})	0.031	0.020	−0.464	0.677	0.416	0.002	0.400	0.369	0.01	0.70
	Contribution (× 10^{-4})	0.050	0.153	−4.048	0.002	0.002	> 0.001	0.005	0.008	0.01	0.40

Note that residual variance was not calculated for response variable with binary distribution (GRO occurrence).
Int, intercept.

greater than the variance in temperature slope, indicating stronger tree-specific sensitivity to VPD compared to temperature (Q4).

Discussion

Although intra-annual growth dynamics of coexisting broadleaved species respond to the same environmental variables of temperature and VPD, the overall intra-annual growth patterns largely differ between species. The radial increment of all three species is driven mainly by highly effective growth close to temperatures and VPD values of around 14°C and ≤ 0.1 kPa, respectively (Figs 4, 5). Both radial growth rates and occurrence of days with radial growth peak inside this climatic optimum and, consequently, growth during this optimum contributes the most to annual ring width. *Fagus sylvatica* and *A. pseudoplatanus* were adapted to partly sustain radial growth also in conditions with suboptimal VPD and contributed significantly to annual growth also during VPD > 0.1 kPa (Fig. 4). By contrast, growth during VPD > 0.1 kPa was considerably lower for *Q. robur*. This was reflected in prominent differences in intra-annual radial growth patterns between unimodal with a single peak of growth rates in both diffuse-porous broadleaves and flat multimodal in the ring-porous *Q. robur* (Fig. 2).

Response of radial growth to climatic factors

The observed responses of growth rates to climatic conditions are in line with existing experimental and empirical knowledge (Ziaco & Biondi, 2018; Güney *et al.*, 2020; Zweifel *et al.*, 2021). Most importantly, the growth rate peaked during periods of full air moisture saturation (VPD = 0 kPa) and between 47% and 68% of the tree ring was formed under fully saturated or weakly dry conditions (VPD < 0.1 kPa; Fig. 4). This reflects the predominant control of turgor pressure over radial growth (Zweifel *et al.*, 2005; Peters *et al.*, 2021). Turgor affects radial growth mainly through alterations of the rate of cambial cells' division (Cuny *et al.*, 2015). The frequency of cambial cells division depends on the speed of their radial growth and the level of cell wall relaxation, which is mechanically forced by turgor pressure

(Vaganov *et al.*, 2006; Cabon *et al.*, 2020). Accordingly, the 'zero-growth approach' employed in this study assumes that radial growth cannot be sustained if the tree water status is suboptimal (Güney *et al.*, 2020; Krejza *et al.*, 2021), which was also confirmed empirically (Zweifel *et al.*, 2016). Consequently, the growth rate peaked at timestamps with optimal or slightly suboptimal VPD, mainly at night after replenishment of the stem water content (Fig. S4; Zweifel *et al.*, 2021).

We observed a stronger coupling of radial growth to relative air humidity and VPD compared to soil moisture availability (Fig. 3). This suggests a stronger dependence of the stem water balance on moisture losses through transpiration compared to the limitation of water uptake by the root system (Zweifel *et al.*, 2005; Oberhuber & Gruber, 2010; Siegmund *et al.*, 2016). This can translate into a direct response of xylogenesis to air but not to soil humidity (Morino *et al.*, 2021) leading to a limited capacity of soil moisture to buffer the negative effects of increasing VPD on tree growth (Grossiord *et al.*, 2020). The overall dependency of sub-daily growth rates on soil water potential is known to be weak in broadleaves compared to conifers (Zweifel *et al.*, 2021). Moreover, the considerable growth of *A. pseudoplatanus* observed under very dry soil conditions (Fig. 4b,c) confirms an indirect, temporarily unstable and strongly nonlinear response of sub-daily radial growth to soil water potential (Zweifel *et al.*, 2021).

Radial growth rates showed an air temperature optimum between 12 and 18°C with declining growth both for higher and lower temperatures. Although cambial activity was sustained through a wide temperature range between 0 and 40°C under experimental conditions (Cabon *et al.*, 2020), it became strongly limited by a low rate of cambial cells division below 5–8°C (Körner, 2012). A similar threshold of mean air temperature is also required before spring cambial reactivation from dormancy (Rossi *et al.*, 2008b; Prislan *et al.*, 2013) and represents the minimum mean growing season temperature required for tree survival (Körner, 2012). Indeed, we observed a drop in all growth variables below 10°C (Fig. 4). Cumulative growth below this threshold contributed less to total annual growth than was the proportion of 30-min timestamps with temperatures below 10°C. The dominant contribution of growth around 14°C to total annual growth is in accordance with process-based

modelling studies, which calibrated lower margins of the temperature optimum for European woody species between 11 and 16°C (Touchan *et al.*, 2012; Tumajer *et al.*, 2017; Jevšenak *et al.*, 2021; Kašpar *et al.*, 2021), and empirical observations of a decoupling or inverting of temperature–growth correlations above 13–13.5°C (Carrer *et al.*, 1998; Sidor *et al.*, 2015).

Differences in the climate–radial growth interaction and growth patterns between species

While the overall pattern of temperature and VPD limitation of radial growth was similar for all the species, with a growth peak under warm and wet conditions, we observed a steeper reduction of growth rates with declining humidity for *Q. robur* compared to *A. pseudoplatanus* and *F. sylvatica* (Figs 4a, 5a). Anisohydric oaks can maintain transpiration during more negative water potentials (Scherrer *et al.*, 2011). However, they probably experience more intensive radial shrinking of the stem caused by a tree water deficit and might therefore not be able to grow under increased VPD. A large vessel lumen area prioritizing water conductivity results in lower cavitation resistance under drought stress in ring-porous species (Pallardy, 2008; Sperry *et al.*, 2008). Moreover, the cessation of radial growth caused by summer drought stress might be more detrimental for oaks compared to beech, because oaks are less able to refill large cavitated vessels and to reactivate cambial growth during wetter autumn periods (van der Werf *et al.*, 2007).

Alternatively, the observed differences between species in growth across the range of environmental conditions (Fig. 4c) might mirror differences in leaf and cambial phenology. Ring-porous species partly compensate for their sensitivity to VPD by an early onset of cambial activity (D'Orangeville *et al.*, 2021). The formation of the first xylem layers occurs before leaf unfolding in *Q. robur* (Sass-Klaassen *et al.*, 2011) when the stem water content is not negatively affected by stomatal transpiration. Indeed, growth rates tend to respond positively to increasing temperature and show weak dependence on VPD during early spring in *Q. robur*, but not in diffuse-porous species under study (Fig. 3). This might contribute to a lower proportion of growth under VPD > 0.1 kPa in *Q. robur* compared to diffuse-porous species and explain different correlations with May climatic conditions. An early onset of cambial activity might offset the negative effects of the *Q. robur* sensitivity to summer VPD on annual tree ring width. Indeed, dendrochronological studies from our study region have found a significantly stronger drought limitation of annual radial growth for *F. sylvatica* compared to *Q. robur* (Scharnweber *et al.*, 2011; Vanhellemont *et al.*, 2019).

Visually as well statistically, both diffuse-porous species always experienced a unimodal growth pattern with a single peak mostly during June. By contrast, the growth dynamics of *Q. robur* statistically lacked the single global peak in five of the six years, and a flat multimodal distribution with a single global peak and multiple local peaks only occurred in 2020 (Fig. 2). The kurtosis and skewness of intra-annual growth rates were always lowest for *Q. robur*, suggesting a flat distribution with an indistinct global maximum around the middle of the growing season. In addition, the proportions of growing trees showed mostly continuous trends over the growing season for *F. sylvatica* and *A. pseudoplatanus* whereas abrupt day-to-day oscillations occurred in the case of *Q. robur*. We suggest that the different intra-annual growth patterns of coexisting species reflect their different VPD sensitivity. The great contribution of intervals of optimal VPD to total growth and very low growth rates under suboptimal VPD (0.1–0.5 kPa) of *Q. robur* (Fig. 4) result in the more frequent abrupt reductions or even cessations of cambial activity during dry parts of the growing season compared to diffuse-porous broadleaves. Consequently, the intra-annual growth pattern of *Q. robur* becomes flat, frequently discontinuous and very 'spiky'.

Species-specific growth dynamics during the growing season might challenge the appropriateness of some statistics frequently employed for analysis of dendrometer data. For instance, detrending of the dendrometer data using the so-called 'daily' approach assumes steady growth during the entire growing season, which can be approximated using the Gompertz equation (van der Maaten *et al.*, 2016) or generalized additive models (Cuny *et al.*, 2013). Although the intra-annual pattern of tree-ring formation does not differ in the case of 'zero growth' and 'daily' approaches applied to our dataset (Fig. S5), steadily increasing functions might fail to reflect growth variability in the Mediterranean and semi-arid regions with prolonged periods of growth cessation (Campelo *et al.*, 2018; Ziaco & Biondi, 2018). Similarly, steadily increasing functions seem to be more suitable growth models for *A. pseudoplatanus* and *F. sylvatica* compared to *Q. robur* coexisting in temperate mixed forests.

Radial growth variability among trees

Very low values of marginal (R^2m) compared to conditional (R^2c) pseudo-R^2 in mixed-effects models suggested large differences in climatic sensitivity of individual trees. For instance, according to combined tree-specific slopes (fixed + random), an increase of VPD of 0.1 kPa can trigger a drop in growth rates of between -0.014 and -0.109 μm h^{-1}, depending on the tree individual. Between-tree variability in climate–growth response in mixed uneven-aged stands might be a reflection of plant ontogenetic development (Rossi *et al.*, 2008a; Konter *et al.*, 2016), tree morphology (Trouillier *et al.*, 2019) or social status (Mérian & Lebourgeois, 2011). The prominent difference in climatic sensitivity at a sub-daily scale could then partly explain diverging multidecadal growth trends of coexisting trees in response to the same climate change (Buras *et al.*, 2016). In the case of our dataset, the between-tree variability in climatic sensitivity might be partly given by the heterogeneity of soil conditions between the three monitoring plots (Scharnweber *et al.*, 2020), which might alter radial growth through the availability of soil moisture (van der Werf *et al.*, 2007). According to random intercepts of mixed-effects models, trees at the Vilm island site tend to grow at a lower pace compared to both inland sites (Table S4). However, performing individual analyses separately for each of the three monitoring sites yielded virtually homogenous results in terms of climate–growth interaction (not shown), confirming the

robustness of the observed VPD control over radial growth (Güney *et al.*, 2020; Zweifel *et al.*, 2021).

Anticipated growth dynamics under ongoing climate change and during climatically extreme years

The mean temperature and VPD during the main growing season at our site equalled 13.2°C and 0.29 kPa, respectively. In light of our results, the mean temperature can be considered very close to the climatic optimum with a peak of growth rates, occurrence and contribution to total growth for all the species (Fig. 5). However, the mean VPD clearly represents suboptimal conditions, allowing growth mainly at night (Fig. S4; Zweifel *et al.*, 2021). According to ensemble predictions, the region of the Baltic coast is expected to be warmer by 3.5–4.5°C at the end of the 21st century compared to 1970–1999 (Boé *et al.*, 2020). The forecasted increase of mean growing season temperature to about 16–18°C might not directly restrict tree growth, because this temperature range still permits very effective radial growth (Fig. 4). By contrast, the associated increase of VPD triggered by increasing evaporative demands (Grossiord *et al.*, 2020) and seasonal redistribution of precipitation (Boé *et al.*, 2020) will probably further reinforce its control over radial growth dynamics. Under the conditions of strong VPD limitation, the growth patterns might be expected to further shift from unimodal to multimodal. Cambial phenology and the ability to shift growth into periods with limited transpiration might become – similarly as in the Mediterranean (Cherubini *et al.*, 2003) – an important trait codetermining species performance in mixed forest stands.

The leading role of moisture availability for the future growth of broadleaved woodlands was further highlighted by the growth response to the recent summer drought events. For instance, a reduced rate of radial growth was observed for all species during the dry 2019 growing season (Fig. 2; Table S3), when drought stress was further amplified by legacy effects (e.g. depleted soil water content) after the dry 2018 summer (Scharnweber *et al.*, 2020). Lowland temperate forests represent a transitional ecosystem between cold-limited boreal or mountain forests and drought-limited Mediterranean or steppe woodlands. This determines complex growth responses to the interaction of temperature and moisture availability (Tumajer *et al.*, 2017; Cienciala *et al.*, 2018). In agreement with this, years of extreme growth reductions observed across Central Europe were initiated by a wide spectrum of climatic drivers; however, warm and dry conditions seem to be the leading mechanism in the lowlands (Neuwirth *et al.*, 2007). Consequently, a mechanistic understanding of complex, nonlinear and possibly nonstationary interactions between temperature, moisture and their legacy effects is necessary to predict the response of intra-annual and diurnal growth to current climatic extremes (Vaganov *et al.*, 2006; Zweifel *et al.*, 2021).

Conclusions

The annual radial increment of the three temperate broadleaved species under study is driven mainly by intensive growth in periods with air temperatures of around 14°C and a VPD below 0.1 kPa. The reduction of radial growth rates caused by suboptimal moisture tends to be more pronounced in *Q. robur* compared to *A. pseudoplatanus* and *F. sylvatica*. This shapes the typical growth pattern during the growing season, which in the case of *Q. robur* lacks a single peak during summer but rather responds to individual events of high humidity. By contrast, intra-annual growth rates of *A. pseudoplatanus* and *F. sylvatica* show a distinct peak around DOY 150–170.

Although all the trees of all three species showed robust climatic responses of growth rates, the slopes of these responses indicated significant differences between individual trees. This suggests that specific internal (ontogenetic development, morphology), external (microsite) or legacy factors (preceding climatic events) strongly modulate the effect of the macroclimate on intra-annual growth dynamics. This challenges predictions of future dynamics of European temperate broadleaved forests and highlights the greater resilience of heterogeneous populations, as individuals of the same species seem to be adapted to different climatic niches. A large number of individuals with continuous monitoring of radial growth or massive application of process-based models capable of simulating intra-annual growth dynamics will be required to decipher all sources of random variability on growth dynamics at the landscape scale.

Author contributions

TS, MS and MW designed, established, and maintained plots of forest growth monitoring and associated databases. MS performed quality control and pre-processing of the datasets. JT performed the analyses and led the writing of the manuscript with significant input from the other co-authors. All co-authors approved the final version of the manuscript.

ORCID

Tobias Scharnweber https://orcid.org/0000-0002-4933-5296
Marko Smiljanic https://orcid.org/0000-0002-2324-0723
Jan Tumajer https://orcid.org/0000-0002-7773-7081
Martin Wilmking https://orcid.org/0000-0003-4964-2402

Data availability

The data that support the findings of this study are available from the corresponding author upon reasonable request.

References

Ameijeiras-Alonso J, Crujeiras RM, Rodriguez-Casal A. 2021. MULTIMODE: an R package for mode assessment. *Journal of Statistical Software* **97**: 1–32.

Anderegg WRL, Klein T, Bartlett M, Sack L, Pellegrini AFA, Choat B, Jansen S. 2016. Meta-analysis reveals that hydraulic traits explain cross-species patterns of drought-induced tree mortality across the globe. *Proceedings of the National Academy of Sciences, USA* **113**: 5024–5029.

Babst F, Bouriaud O, Poulter B, Trouet V, Girardin MP, Frank DC. 2019. Twentieth century redistribution in climatic drivers of global tree growth. *Science Advances* **5**: eaat4313.

Backes K, Leuschner C. 2000. Leaf water relations of competitive *Fagus sylvatica* and *Quercus petraea* trees during 4 years differing in soil drought. *Canadian Journal of Forest Research* **30**: 335–346.

Bates D, Mächler M, Bolker B, Walker S. 2015. Fitting linear mixed-effects models using LME4. *Journal of Statistical Software* **67**: 1–48.

Becklin KM, Anderson JT, Gerhart LM, Wadgymar SM, Wessinger CA, Ward JK. 2016. Examining plant physiological responses to climate change through an evolutionary lens. *Plant Physiology* **172**. doi: 10.1104/pp.16.00793.

Boé J, Somot S, Corre L, Nabat P. 2020. Large discrepancies in summer climate change over Europe as projected by global and regional climate models: causes and consequences. *Climate Dynamics* **54**: 2981–3002.

Buras A, van der Maaten-Theunissen M, van der Maaten E, Ahlgrimm S, Hermann P, Simard S, Heinrich I, Helle G, Unterseher M, Schnittler M et al. 2016. Tuning the voices of a choir: detecting ecological gradients in time-series populations. *PLoS ONE* **11**: e0158346.

Cabon A, Peters RL, Fonti P, Martínez-Vilalta J, De Cáceres M. 2020. Temperature and water potential co-limit stem cambial activity along a steep elevational gradient. *New Phytologist* **226**: 1325–1340.

Camarero JJ, Gazol A, Sangüesa-Barreda G, Oliva J, Vicente-Serrano SM. 2015. To die or not to die: early warnings of tree dieback in response to a severe drought. *Journal of Ecology* **103**: 44–57.

Campelo F, Gutiérrez E, Ribas M, Sánchez-Salguero R, Nabais C, Camarero JJ. 2018. The facultative bimodal growth pattern in *Quercus ilex* – a simple model to predict sub-seasonal and inter-annual growth. *Dendrochronologia* **49**: 77–88.

Carrer M, Anfodillo T, Urbinati C, Carraro V. 1998. High-altitude forest sensitivity to global warming: results from long-term and short-term analyses in the Eastern Italian Alps. In: Beniston M, Innes JL, eds. *The impacts of climate variability on forests.* Berlin/Heidelberg, Germany: Springer-Verlag, 171–189.

Cherubini P, Gartner BL, Tognetti R, Bräker OU, Schoch W, Innes JL. 2003. Identification, measurement and interpretation of tree rings in woody species from Mediterranean climates. *Biological Reviews of the Cambridge Philosophical Society* **78**: 119–148.

Ciais PH, Reichstein M, Viovy N, Granier A, Ogée J, Allard V, Aubinet M, Buchmann N, Bernhofer C, Carrara A et al. 2005. Europe-wide reduction in primary productivity caused by the heat and drought in 2003. *Nature* **437**: 529–533.

Cienciala E, Altman J, Doležal J, Kopáček J, Štěpánek P, Ståhl G, Tumajer J. 2018. Increased spruce tree growth in Central Europe since 1960s. *Science of the Total Environment* **619–620**: 1637–1647.

Cook ER, Solomina O, Matskovsky V, Cook BI, Agafonov L, Berdnikova A, Dolgova E, Karpukhin A, Knysh N, Kulakova M et al. 2020. The European Russia drought atlas (1400–2016 CE). *Climate Dynamics* **54**: 2317–2335.

Cuny HE, Rathgeber CBK, Kiessé TS, Hartmann FP, Barbeito I, Fournier M. 2013. Generalized additive models reveal the intrinsic complexity of wood formation dynamics. *Journal of Experimental Botany* **64**: 1983–1994.

Cuny HE, Rathgeber CBK, Frank D, Fonti P, Mäkinen H, Prislan P, Rossi S, del Castillo EM, Campelo F, Vavrčík H et al. 2015. Woody biomass production lags stem-girth increase by over one month in coniferous forests. *Nature Plants* **1**: 15160.

D'Orangeville L, Itter M, Kneeshaw D, Munger JW, Richardson AD, Dyer JM, Orwig DA, Pan Y, Pederson N. 2021. Peak radial growth of diffuse-porous species occurs during periods of lower water availability than for ring-porous and coniferous trees. *Tree Physiology.* doi: 10.1093/treephys/tpab101.

Deslauriers A, Rossi S, Anfodillo T. 2007. Dendrometer and intra-annual tree growth: what kind of information can be inferred? *Dendrochronologia* **25**: 113–124.

Deslauriers A, Rossi S, Anfodillo T, Saracino A. 2008. Cambial phenology, wood formation and temperature thresholds in two contrasting years at high altitude in southern Italy. *Tree Physiology* **28**: 863–871.

Drew DM, Downes GM. 2009. The use of precision dendrometers in research on daily stem size and wood property variation: a review. *Dendrochronologia* **27**: 159–172.

Duursma RA. 2015. Plantecophys – an R package for analysing and modelling leaf gas exchange data. *PLoS ONE* **10**: e0143346.

Grossiord C, Buckley TN, Cernusak LA, Novick KA, Poulter B, Siegwolf RTW, Sperry JS, McDowell NG. 2020. Plant responses to rising vapor pressure deficit. *New Phytologist* **226**: 1550–1566.

Güney A, Zweifel R, Türkan S, Zimmermann R, Wachendorf M, Güney CO. 2020. Drought responses and their effects on radial stem growth of two co-occurring conifer species in the Mediterranean mountain range. *Annals of Forest Science* **77**: 105.

Huang J-G, Ma Q, Rossi S, Biondi F, Deslauriers A, Fonti P, Liang E, Mäkinen H, Oberhuber W, Rathgeber CBK et al. 2020. Photoperiod and temperature as dominant environmental drivers triggering secondary growth resumption in Northern Hemisphere conifers. *Proceedings of the National Academy of Sciences, USA* **117**: 20645–20652.

Jevšenak J, Tychkov I, Gričar J, Levanič T, Tumajer J, Prislan P, Arnič D, Popkova M, Shishov VV. 2021. Growth-limiting factors and climate response variability in Norway spruce (*Picea abies* L.) along an elevation and precipitation gradients in Slovenia. *International Journal of Biometeorology* **65**: 311–324.

Kang Y-J, Noh Y. 2019. Development of Hartigan's dip statistic with bimodality coefficient to assess multimodality of distributions. *Mathematical Problems in Engineering* **2019**: 1–17.

Kašpar J, Tumajer J, Šamonil P, Vašíčková I. 2021. Species-specific climate–growth interactions determine tree species dynamics in mixed Central European mountain forests. *Environmental Research Letters* **16**: 034039.

King G, Fonti P, Nievergelt D, Büntgen U, Frank D. 2013. Climatic drivers of hourly to yearly tree radius variations along a 6°C natural warming gradient. *Agricultural and Forest Meteorology* **168**: 36–46.

Konter O, Büntgen U, Carrer M, Timonen M, Esper J. 2016. Climate signal age effects in boreal tree-rings: lessons to be learned for paleoclimatic reconstructions. *Quaternary Science Reviews* **142**: 164–172.

Körner C. 2012. Treelines will be understood once the functional difference between a tree and a shrub is. *Ambio* **41**: 197–206.

Körner C. 2018. Concepts in empirical plant ecology. *Plant Ecology & Diversity* **11**: 405–428.

Krejza J, Cienciala E, Světlík J, Bellan M, Noyer E, Horáček P, Štěpánek P, Marek MV. 2021. Evidence of climate-induced stress of Norway spruce along elevation gradient preceding the current dieback in Central Europe. *Trees* **35**: 103–119.

Lévesque M, Saurer M, Siegwolf R, Eilmann B, Brang P, Bugmann H, Rigling A. 2013. Drought response of five conifer species under contrasting water availability suggests high vulnerability of Norway spruce and European larch. *Global Change Biology* **19**: 3184–3199.

van der Maaten E, van der Maaten-Theunissen M, Smiljanić M, Rossi S, Simard S, Wilmking M, Deslauriers A, Fonti P, von Arx G, Bouriaud O. 2016. DENDROMETER: analyzing the pulse of trees in R. *Dendrochronologia* **40**: 12–16.

van der Maaten E, Pape J, van der Maaten-Theunissen M, Scharnweber T, Smiljanić M, Cruz-García R, Wilmking M. 2018. Distinct growth phenology but similar daily stem dynamics in three co-occurring broadleaved tree species. *Tree Physiology* **38**: 1820–1828.

Mérian P, Lebourgeois F. 2011. Size-mediated climate–growth relationships in temperate forests: a multi-species analysis. *Forest Ecology and Management* **261**: 1382–1391.

Morino K, Minor RL, Barron-Gafford GA, Brown PM, Hughes MK. 2021. Bimodal cambial activity and false-ring formation in conifers under a monsoon climate. *Tree Physiology* 41: 1893–1905.

Nakagawa S, Schielzeth H. 2013. A general and simple method for obtaining R^2 from generalized linear mixed-effects models. *Methods in Ecology and Evolution* 4: 133–142.

Neuwirth B, Schweingruber FH, Winiger M. 2007. Spatial patterns of central European pointer years from 1901 to 1971. *Dendrochronologia* 24: 79–89.

Oberhuber W, Gruber A. 2010. Climatic influences on intra-annual stem radial increment of *Pinus sylvestris* (L.) exposed to drought. *Trees* 24: 887–898.

Pallardy SG. 2008. *Physiology of woody plants*. New York, NY, USA: Elsevier.

Pan Y, Birdsey RA, Fang J, Houghton R, Kauppi PE, Kurz WA, Phillips OL, Shvidenko A, Lewis SL, Canadell JG et al. 2011. A large and persistent carbon sink in the world's forests. *Science* 333: 988–993.

Peñuelas J, Rutishauser T, Filella I. 2009. Phenology feedbacks on climate change. *Science* 324: 887–888.

Pérez-de-Lis G, Rossi S, Vázquez-Ruiz RA, Rozas V, García-González I. 2016. Do changes in spring phenology affect earlywood vessels? Perspective from the xylogenesis monitoring of two sympatric ring-porous oaks. *New Phytologist* 209: 521–530.

Peters RL, Steppe K, Cuny HE, De Pauw DJW, Frank DC, Schaub M, Rathgeber CBK, Cabon A, Fonti P. 2021. Turgor – a limiting factor for radial growth in mature conifers along an elevational gradient. *New Phytologist* 229: 213–229.

Prislan P, Gričar J, de Luis M, Smith KT, Čufar K. 2013. Phenological variation in xylem and phloem formation in *Fagus sylvatica* from two contrasting sites. *Agricultural and Forest Meteorology* 180: 142–151.

R Core Team. 2020. *R: a language and environment for statistical computing (v.4.1.1.)*. Vienna, Austria: R Foundation for Statistical Computing.

Rossi S, Anfodillo T, Čufar K, Cuny HE, Deslauriers A, Fonti P, Frank D, Gričar J, Gruber A, Huang J-G et al. 2016. Pattern of xylem phenology in conifers of cold ecosystems at the Northern Hemisphere. *Global Change Biology* 22: 3804–3813.

Rossi S, Deslauriers A, Morin H. 2003. Application of the Gompertz equation for the study of xylem cell development. *Dendrochronologia* 21: 33–39.

Rossi S, Deslauriers A, Anfodillo T, Carrer M. 2008a. Age-dependent xylogenesis in timberline conifers. *New Phytologist* 177: 199–208.

Rossi S, Deslauriers A, Gričar J, Seo JW, Rathgeber CBK, Anfodillo T, Morin H, Levanic T, Oven P, Jalkanen R. 2008b. Critical temperatures for xylogenesis in conifers of cold climates. *Global Ecology and Biogeography* 17: 696–707.

Sass-Klaassen U, Sabajo CR, den Ouden J. 2011. Vessel formation in relation to leaf phenology in peduncuate oak and European ash. *Dendrochronologia* 29: 171–175.

Scharnweber T, Manthey M, Criegee C, Bauwe A, Schröder C, Wilmking M. 2011. Drought matters – declining precipitation influences growth of *Fagus sylvatica* L. and *Quercus robur* L. in north-eastern Germany. *Forest Ecology and Management* 262: 947–961.

Scharnweber T, Smiljanic M, Cruz-García R, Manthey M, Wilmking M. 2020. Tree growth at the end of the 21st century – the extreme years 2018/19 as template for future growth conditions. *Environmental Research Letters* 15: 074022.

Scherrer D, Bader MK-F, Körner C. 2011. Drought-sensitivity ranking of deciduous tree species based on thermal imaging of forest canopies. *Agricultural and Forest Meteorology* 151: 1632–1640.

Sidor CG, Popa I, Vlad R, Cherubini P. 2015. Different tree-ring responses of Norway spruce to air temperature across an altitudinal gradient in the Eastern Carpathians (Romania). *Trees* 29: 985–997.

Siegmund JF, Sanders TGM, Heinrich I, Van Der Maaten E, Simard S, Helle G, Donner RV. 2016. Meteorological drivers of extremes in daily stem radius variations of beech, oak, and pine in northeastern Germany: an event coincidence analysis. *Frontiers in Plant Science* 7: 1–14.

Silwerman BW. 1981. Using kernel density estimates to investigate multimodality. *Journal of the Royal Statistical Society. Series B: Methodological* 43: 97–99.

Sperry JS, Meinzer FC, McCulloh KA. 2008. Safety and efficiency conflicts in hydraulic architecture: scaling from tissues to trees. *Plant, Cell & Environment* 31: 632–645.

Touchan R, Shishov VV, Meko DM, Nouiri I, Grachev A. 2012. Process based model sheds light on climate sensitivity of Mediterranean tree-ring width. *Biogeosciences* 9: 965–972.

Trouillier M, van der Maaten-Theunissen M, Scharnweber T, Würth D, Burger A, Schnittler M, Wilmking M. 2019. Size matters—a comparison of three methods to assess age- and size-dependent climate sensitivity of trees. *Trees* 33: 183–192.

Tumajer J, Altman J, Štěpánek P, Treml V, Doležal J, Cienciala E. 2017. Increasing moisture limitation of Norway spruce in Central Europe revealed by forward modelling of tree growth in tree-ring network. *Agricultural and Forest Meteorology* 247: 56–64.

Vaganov EA, Hughes MK, Shashkin AV. 2006. *Growth dynamics of conifer tree rings: images of past and future environments*. Berlin/Heidelberg, Germany: Springer-Verlag.

Vanhellemont M, Sousa-Silva R, Maes SL, Van den Bulcke J, Hertzog L, De Groote SRE, Van Acker J, Bonte D, Martel AN, Lens L et al. 2019. Distinct growth responses to drought for oak and beech in temperate mixed forests. *Science of the Total Environment* 650: 3017–3026.

Walthert L, Ganthaler A, Mayr S, Saurer M, Waldner P, Walser M, Zweifel R, von Arx G. 2021. From the comfort zone to crown dieback: sequence of physiological stress thresholds in mature European beech trees across progressive drought. *Science of the Total Environment* 753: 141792.

van der Werf GW, Sass-Klaassen UGW, Mohren GMJ. 2007. The impact of the 2003 summer drought on the intra-annual growth pattern of beech (*Fagus sylvatica* L.) and oak (*Quercus robur* L.) on a dry site in the Netherlands. *Dendrochronologia* 25: 103–112.

Wickham H. 2009. GGPLOT2: elegant graphics for data analysis. New York, NY, USA: Springer-Verlag.

Wilmking M, Maaten-Theunissen M, Maaten E, Scharnweber T, Buras A, Biermann C, Gurskaya M, Hallinger M, Lange J, Shetti R et al. 2020. Global assessment of relationships between climate and tree growth. *Global Change Biology* 26: 3212–3220.

Wu M, Liu N, Bao G, Gao J. 2020. Climatic factors of radial growth of *Pinus tabulaeformis* in eastern Gansu, northwest China based on Vaganov-Shashkin model. *Geografiska Annaler. Series A: Physical Geography* 102: 196–208.

Ziaco E, Biondi F. 2018. Stem circadian phenology of four pine species in naturally contrasting climates from sky-island forests of the western USA. *Forests* 9: 396.

Zweifel R, Haeni M, Buchmann N, Eugster W. 2016. Are trees able to grow in periods of stem shrinkage? *New Phytologist* 211: 839–849.

Zweifel R, Häsler R. 2000. Frost-induced reversible shrinkage of bark of mature subalpine conifers. *Agricultural and Forest Meteorology* 102: 213–222.

Zweifel R, Sterck F, Braun S, Buchmann N, Eugster W, Gessler A, Häni M, Peters RL, Walthert L, Wilhelm M et al. 2021. Why trees grow at night. *New Phytologist* 231: 2174–2185.

Zweifel R, Zimmermann L, Newbery DM. 2005. Modeling tree water deficit from microclimate: an approach to quantifying drought stress. *Tree Physiology* 25: 147–156.

Supporting Information

Additional Supporting Information may be found online in the Supporting Information section at the end of the article.

Fig. S1 Scatterplots of mean growth rates across air temperatures and vapour pressure deficits for specific years.

Fig. S2 Scatterplots of growth occurrence across air temperatures and vapour pressure deficits for specific years.

Fig. S3 Scatterplots of growth contribution across air temperatures and vapour pressure deficits for specific years.

Fig. S4 Mean growth rates for individual 30-min intervals during the day.

Fig. S5 Comparison of intra-annual patterns of increasing stem radius estimated using the daily and zero-growth model.

Table S1 Proportions of trees per species with significant intra-annual growth multimodality.

Table S2 Fixed, random, and combined effects of slopes of climatic variables in the mixed-effects models for individual trees.

Table S3 Fixed and random effects on intercepts in the mixed-effects models for individual years.

Table S4 Random effects on intercepts in the mixed-effects models for individual trees.

Please note: Wiley Blackwell are not responsible for the content or functionality of any Supporting Information supplied by the authors. Any queries (other than missing material) should be directed to the *New Phytologist* Central Office.

About *New Phytologist*

- *New Phytologist* is an electronic (online-only) journal owned by the New Phytologist Foundation, a **not-for-profit organization** dedicated to the promotion of plant science, facilitating projects from symposia to free access for our Tansley reviews and Tansley insights.

- Regular papers, Letters, Viewpoints, Research reviews, Rapid reports and both Modelling/Theory and Methods papers are encouraged. We are committed to rapid processing, from online submission through to publication 'as ready' via *Early View* – our average time to decision is <23 days. There are **no page or colour charges** and a PDF version will be provided for each article.

- The journal is available online at Wiley Online Library. Visit **www.newphytologist.com** to search the articles and register for table of contents email alerts.

- If you have any questions, do get in touch with Central Office (np-centraloffice@lancaster.ac.uk) or, if it is more convenient, our USA Office (np-usaoffice@lancaster.ac.uk)

- For submission instructions, subscription and all the latest information visit **www.newphytologist.com**